Formation energy puzzle in intermetallic alloys: Random phase approximation fails to predict accurate formation energies

Niraj K. Nepal,* Santosh Adhikari, Bimal Neupane, and Adrienn Ruzsinszky
Department of Physics, Temple University, Philadelphia, Pennsylvania 19122, USA

(Received 21 July 2020; accepted 2 November 2020; published 19 November 2020)

We performed density-functional calculations to estimate the formation energies of intermetallic alloys. We used two semilocal approximations, the generalized gradient approximation (GGA) by Perdew-Burke-Ernzerhof (PBE), and the strongly constrained and appropriately normed (SCAN) meta-GGA. In addition, we utilized two nonlocal DFT functionals, the hybrid HSE06, and the state-of-the-art random phase approximation (RPA). The nonlocal functionals such as HSE06 and RPA yield accurate formation energies of binary alloys with completely filled d-band metals, where semilocal functionals underperform. The accuracy of the nonlocal functionals is greatly reduced when a partially filled d-band metal is present in an alloy, while PBE-GGA outperforms in these cases. We show that the accurate prediction of formation energies by any DFT method depends on its ability to predict the accurate electronic properties, e.g., valence d-band contribution to the density of states (DOS). The SCAN meta-GGA often corrects the PBE-DOS, however, it does not provide accurate formation energies compared to PBE. This is assumed to be due to the lack of proper error cancellation that should be expected due to the similar bulk nature of both alloys and their constituents, which may improve with the modification of meta-GGA ingredients. RPA yields too-negative formation energies of alloys with partially filled d-band metals. RPA results can be corrected by restoring the exchange-correlation kernel, thereby improving the short-range electron-electron correlation in metallic densities.

DOI: 10.1103/PhysRevB.102.205121

I. INTRODUCTION

Intermetallic alloys, composed of two or more d-band transition metals, are often interesting for applications, therefore, their application-governed aspects have been mostly explored. In most cases, alloys were classified with respect to various factors such as the radius ratio of two constituents, electronegativity, principle quantum number, ionicity, coordination number, etc. [1–4]. However, there is a scarcity of sufficient information about the chemical bonding and its relation with the equilibrium properties such as formation energy in both theory and experiment [1]. Recently, Zhang *et al.* [5], using DFT calculations [6,7] for the Au–Cu alloys, showed that the accurate prediction of formation energy accompanies an accurate prediction of the density of states (DOS). Here, we will generalize this result using a more diverse set of compounds.

Intermetallic alloys have always been critical tests for various approximations within density-functional theory (DFT). The accurate prediction of basic equilibrium properties of intermetallic alloys and their bulk transition metal constituents with many popular DFT approximations is difficult. Semi (local) approximations such as the local density approximation (LDA) [7] and various generalized gradient approximations (GGAs) are unable to provide accurate formation energy (heat of formation, E_f) of weakly bonded (WB) systems such as Au–Cu alloys [5,8–10]. Incorporating an amount of nonlocality by the kinetic energy density $\tau(r)$, meta-GGAs slightly improve the equilibrium properties including formation energies of Au-Cu alloys [10], but fail to improve beyond PBE [11] when dealing with the more strongly bonded (SB) systems such as HfOs and PtSc [12]. Attempts at correcting the semilocal results with zero-point vibration energy, additive long-range van der Waals (vdW) interaction, and spin-orbit coupling couldn't improve the result for Au-Cu alloys [10].

In general, hybrid functionals within the generalized Kohn-Sham theory that mix the nonlocal exact exchange with DFT exchange do not provide accurate equilibrium properties of bulk transition metals [13]. However, surprisingly, the hybrid HSE06 [14,15] shows some promise in the prediction of the lattice constants and formation energies of WB systems [5]. HSE06 couldn't provide a reasonable bulk modulus, which is a fundamental physical quantity describing the response of the system to external compression or expansion [10]. On the other hand, the random phase approximation (RPA) [16–18] within the adiabatic-connection fluctuation-dissipation theorem [19,20] predicted excellent equilibrium properties including bulk moduli of the Au–Cu alloys [10]. The accurate formation energy of WB systems by these methods may be due to the nonlocality present in them [5,10]. On the contrary, we will later show that such nonlocality is not useful for SB systems; it improves the equilibrium volume but cannot correct the bulk moduli and formation energies.

Many of the earlier works focused mainly on the WB intermetallic alloys [5,8–10], while a few others have included SB alloys [12,21] using semilocal DFT approximations. In this paper, we have explored a broad spectrum of binary

*Corresponding author; niraj.nepal@temple.edu

TABLE I. Constituent elements and their electronic configuration.

Element	Sc	Cu	Zn	Y	Rh	Pd	Ag	Cd	Hf	Os	Pt	Au
Configuration	$3d^14s^2$	$3d^{10}4s^1$	$3d^{10}4s^2$	$4d^15s^2$	$4d^85s^1$	$4d^{10}$	$4d^{10}5s^1$	$4d^{10}5s^2$	$5d^26s^2$	$5d^66s^2$	$5d^96s^1$	$5d^{10}6s^1$

intermetallic alloys from WB to SB. The experimental formation energies of our test set range from 0.07 to 1.18 eV per atom. Most of the systems taken here are binary alloys that crystallize in the B2 (CsCl) phase. Table I presents the d-band metals with their electronic configurations. We have utilized one DFT approximation each from the different rungs of Perdew's Jacob's ladder [22], except for LDA. The PBE-GGA (Perdew-Burke-Ernzerhof) [11], the strongly constrained and appropriately normed (SCAN) [23], the screened hybrid HSE06 (simply HSE by Heyd, Scuseria, and Ernzerhof) [14,15], and RPA were used as the DFT approximations. Both accuracy and computational cost of these approximations, in general, is in the order of PBE < SCAN < HSE06 < RPA. In this assessment, we aim to present a broader picture regarding the performance of various DFT approximations on these intermetallic alloys, which is missing from earlier works.

We will later classify the alloys into three different classes purely based on the performance of different DFT functionals for predicting formation energies, as shown in Fig. 1. We have a WB region (region I), where nonlocal HSE06 and RPA mostly perform better than semilocal PBE and SCAN. In the intermediate region (region II), HSE06 and PBE work much better than others. Finally, there is the SB region (region III), where the nonlocal HSE06 and RPA severely fail to predict the accurate formation energy, while PBE-GGA outperforms them. Note that the classification performed here only refers to intermetallic alloys and is distinct from the classification adopted in Ref. [12] for alloys in general.

II. COMPUTATIONAL DETAILS

All DFT calculations were carried out using a projector augmented wave (PAW) [24] method, as implemented in VASP [25] and GPAW [26–28]. We performed spin-polarized semilocal and HSE06 calculations using VASP, while we used GPAW to perform the RPA calculations. The semilocal calculations were initialized with the magnetic moments per site of 1.5–3.5 μ_B, which converged to the nonmagnetic ground state during self-consistency. However, we obtained the magnetic ground state with a magnetic moment of ~0.5 μ_B in the case of hybrid HSE06 for Pd and Pt. We further confirm that spin-polarized calculations yield more negative energy than the spin-unpolarized ones. The total energy is converged with respect to plane-wave cutoff and k-mesh for all methods within 1–5 meV/atom. In addition, separate convergence tests for the EXX ($E_{\text{total}} - E_c^{\text{RPA}}$) and correlation energies were performed for RPA. The detailed information about the plane-wave cutoff and Brillouin zone sampling are given in Supplemental Material Tables S1 and S2 [29]. Spin-unpolarized ground-state PBE calculations were performed as inputs for the non-self-consistent RPA (for both EXX and correlation energies). We used a maximum cutoff of 350 eV to compute the response function. The correlation energies were computed as a function of the cutoff energy and extrapolated to infinity to get the RPA correlation energy as described in Ref. [30]. The kernel-corrected or beyond RPA (bRPA) calculations were performed at RPA Ecut and a fixed K mesh of 16 x 16 x 16. Also, due to computational complexities, the response function is computed using only one cutoff of 300 eV. We computed formation energies for RPA with and without extrapolation for PtSc with 350 eV, and found a negligible difference of ~ 6 meV per atom. Furthermore, earlier literature also argued that the bRPA methods have a faster convergence with respect to basis set in terms of both maximum cutoff and number of points used in an extrapolation, compared to RPA [31,32]. The gamma point ($\mathbf{q} = 0$) was skipped to avoid the possible divergent contribution and for smooth convergence with respect to k mesh [33], as required for metallic systems. We used the recommended PBE pseudopotentials (PP) modified to include the kinetic energy density for VASP calculations [34], while the 0.9.20000 version of PAW pseudopotentials were utilized for GPAW calculations [27]. The calculations include relativistic effects at the scalar level for each atom within the PAW PP.

Previously, it was shown that the spin-orbit coupling, zero-point vibrational energy, and the nonlocal vdW corrections have negligible effects on the formation energies of intermetallic alloys [10]. Therefore, we did not calculate those corrections in the present assessment. We have performed calculations for seven volume points near the experimental equilibrium volume and fit the Birch-Murnaghan equation of state [35] to evaluate the equilibrium properties. We have used the structures from Ref. [36] and varied the lattice constants isotropically to generate structures with different volumes.

III. RESULTS AND DISCUSSIONS

In this section, we discuss the results for ground-state equilibrium properties of various binary intermetallic alloys and their constituents using DFT calculations. We tabulate and discuss the equilibrium volumes and the bulk moduli in Supplemental Material Tables S3–S6 [29]. The experimental equilibrium volumes and the bulk moduli are presented at room temperature. We notify the reader that the analysis can change quantitatively when the temperature dependence is considered. One can extrapolate the experimental results at room temperature to $T = 0\,\text{K}$ using the linear thermal expansion coefficients [37]. The ZPE slightly changes the equilibrium properties of the metallic systems [38] but is not substantial to alter the overall discussions. Our RPA-calculated equilibrium volumes of bulk elemental constituents are slightly different from those presented in Ref. [38], which is expected, as their results were computed from noisy energy-volume data. On the contrary, our energy-volume data shows a smooth behavior as a result of the tight convergence tests. Unlike equilibrium volumes, the bulk moduli computed from different methods have similar mean absolute error and mean absolute percentage error, with

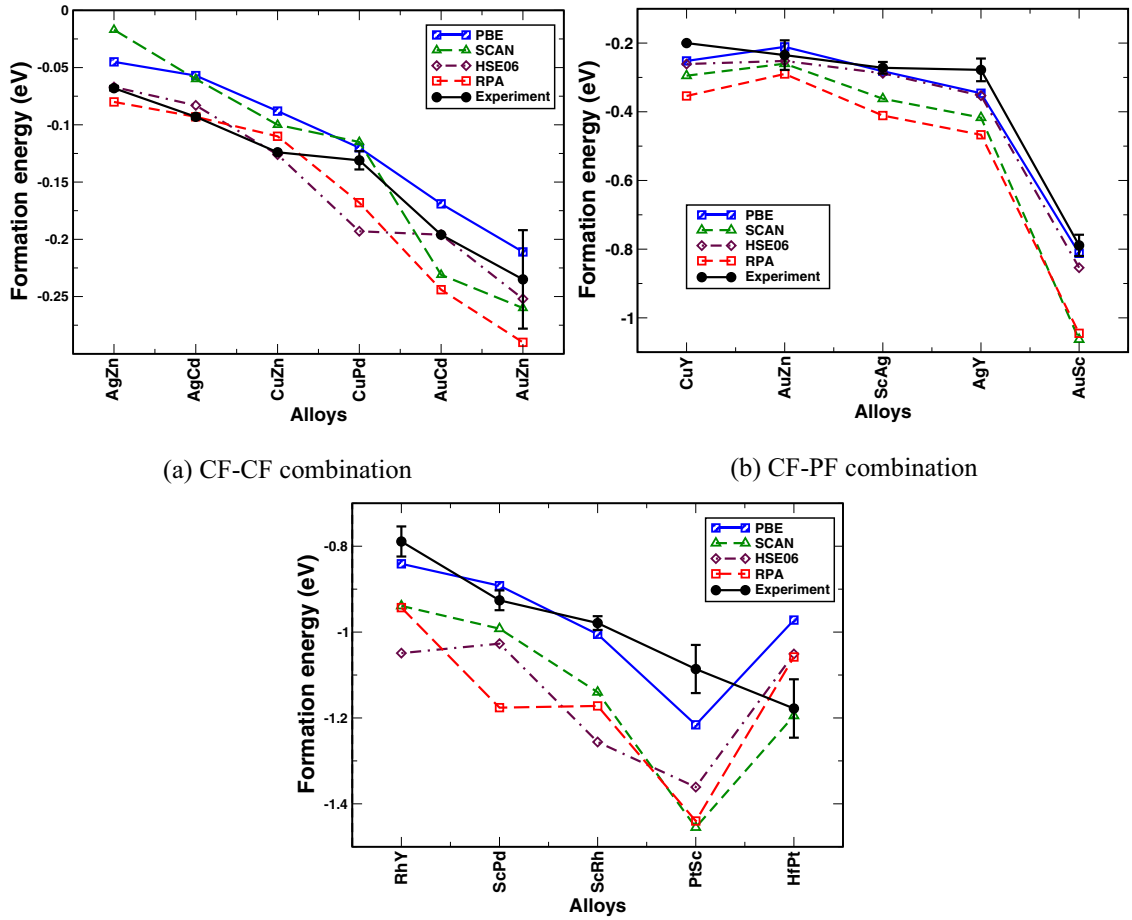

(a) CF-CF combination

(b) CF-PF combination

(c) PF-PF combination

FIG. 1. Formation energies with respect to three distinct classes.

HSE06 and RPA providing a slight improvement over PBE and SCAN.

Here, we mainly focus on the performance of various DFT approximations in predicting formation energies. The formation energy is an important physical quantity in alloy theory as it governs the stability of that alloy. Suppose A_xB_{1-x} is a binary alloy with constituent metals A and B. Then, the formation energy per atom ΔE_f can be computed as

$$\Delta E_f(A_xB_{1-x}) = E(A_xB_{1-x}) - xE(A) - (1-x)E(B), \quad (1)$$

where, $E(A_xB_{1-x})$, $E(A)$, and $E(B)$ are the total bulk energies per atom of an alloy A_xB_{1-x}, metal A and metal B, respectively. x is the fractional weight of metal A in an alloy. A positive formation energy represents an instability, while the negative value depicts the stability of an alloy against its constituents.

We calculated the formation energies using various methods and tabulated the data in Table II. In Table II, we compare the results for an alloy crystallized in the B2 (CsCl) phase with available experimental data. Based on the observation, we classify the results into three distinct categories (or regions), listed below, depending on the filling of d-band in metals, as shown in Fig. 1.

(1) Completely filled/completely filled (CF-CF)
(2) Completely filled/partially filled (CF-PF)
(3) Partially filled/partially filled (PF-PF)

The values are tabulated by an increasing magnitude of experimental formation energies within each section. To understand the performance of functionals on formation energies, we plot the electronic DOS of alloy and its constituents because the structural stability of an alloy is largely dependent on the DOS [1]. We show that an accurate prediction of formation energy should be accompanied by an accurate prediction of the DOS, even for the CF-CF alloys, which have smaller formation energies. In CF metals and CF-CF alloys, the overall position of the d bands may still guide the nature of DOS in the vicinity of the Fermi level that can affect such small formation energies.

A. CF-CF combination

This set consists of intermetallic alloys with constituent bulk metals having completely filled (CF) d bands such as AgZn, AgCd, CuZn, CuPd, AuCd, and AuZn [see Fig. 1(a)]. These weakly bonded alloys have lower experimental formation energies up to 200 meV, compared to other combinations. In this region, the PBE-GGA underestimates the formation energies as expected. The SCAN meta-GGA slightly improves upon PBE and yields mixed results, i.e., underestimates the formation energies for systems AgZn, AgCd, CuZn, and

TABLE II. Formation energy (eV) per atom of intermetallic alloys; the first column represents the alloys, while the second column shows the combination of the d bands; CF is completely filled, PF is partially filled. All the compounds considered here crystallize in the B2 (CsCl) phase.

Alloys	Combination	PBE	SCAN	HSE06	RPA	Experiment
AgZn	4*d*(CF)-3*d*(CF)	−0.045	−0.017	−0.067	−0.080	−0.068 ± 0.002 [39]
AgCd	4*d*(CF)-4*d*(CF)	−0.057	−0.060	−0.083	−0.093	−0.093 ± 0.002 [39]
CuZn	3*d*(CF)-3*d*(CF)	−0.088	−0.100	−0.126	−0.110	−0.124 [39]
CuPd	3*d*(CF)-4*d*(CF)	−0.120	−0.115	−0.193	−0.168	−0.131 ± 0.008 [39]
AuCd	5*d*(CF)-4*d*(CF)	−0.169	−0.231	−0.196	−0.244	−0.196 [39]
AuZn	5*d*(CF)-3*d*(CF)	−0.211	−0.260	−0.252	−0.290	−0.235 ± 0.043 [39]
CuY	3*d*(CF)-4*d*(PF)	−0.252	−0.295	−0.261	−0.354	−0.200 ± 0.002 [40,41]
ScAg	3*d*(PF)-4*d*(CF)	−0.282	−0.362	−0.288	−0.411	−0.272 ± 0.017 [41,42]
AgY	4*d*(CF)-4*d*(PF)	−0.346	−0.417	−0.353	−0.467	−0.278 ± 0.033 [41,42]
AuSc	5*d*(CF)-3*d*(PF)	−0.812	−1.063	−0.854	−1.045	−0.789 ± 0.031 [41,42]
ScPd	3*d*(PF)-4*d*(CF)	−0.892	−0.992	−1.027	−1.176	−0.926 ± 0.023 [41,45]
HfOs	5*d*(PF)-5*d*(PF)	−0.704	−0.754	−0.923	−0.667	−0.482 ± 0.052 [12,43][a]
RhY	4*d*(PF)-4*d*(PF)	−0.841	−0.939	−0.979	−0.943	−0.789 ± 0.035 [41,44]
ScRh	3*d*(PF)-4*d*(PF)	−1.005	−1.140	−1.264	−1.172	−0.979 ± 0.016 [41,45]
PtSc	5*d*(PF)-3*d*(PF)	−1.216	−1.455	−1.382	−1.440	−1.086 ± 0.056 [41,45]
HfPt	5*d*(PF)-5*d*(PF)	−0.972	−1.195	−1.073	−1.058	−1.178 ± 0.068 [41,46]

[a]It is mentioned in the reference that HfOs alloy sample was not completely pure. It had small amounts of $Hf_{54}Os_{17}$ and relatively important quantities of unreacted Os. Therefore, the true result should be more exothermic than −0.518 eV [43].

CuPd, while overestimating them in the cases of AuCd and AuZn. In general, SCAN overestimates the experimental energies below CuPd with a formation energy larger than or equal to 130 meV. On the other hand, the hybrid HSE06 consistently predicts accurate formation energies compared to the experiment, and in agreement with the previous calculations on alloys of CF-CF combination [5]. Our results are also valid for structures other than the B2 phase, which is evident from Table III and Ref. [5]. This indicates that the phase of the crystal has an insignificant role in the performance of DFT approximations when predicting formation energies of intermetallic alloys. To describe the results, we investigate the electronic properties of the alloy and its constituent bulk metals.

We computed valence-state electronic partial density of states (PDOS) for metals having CF d bands and alloys of CF-CF combination and present them in Figures 2 and 3, respectively. The contribution from s and p bands near the Fermi level is negligible (not shown here) compared to that of d band. Therefore, we only show the d-band contribution of the density of states (DOS) and compare it with the experimental PDOS of occupied states. Experimentally, one can obtain information about the valence d band (or PDOS) from x-ray (XPS) or ultraviolet (UPS) photoemission spectra [47–58] (see section Experimental Data for Valence d band in Supplemental Material [29]).

In Fig. 2, we compare the calculated d-band contribution to DOS (PDOS) with experimental d-band ranges extracted from photoemission spectra (Supplemental Material Table S7). We present the PDOS for CF metals such as Cu, Zn, Pd, Ag, Cd, and Au. The negligible density of states at the Fermi level indicates the complete filling of valence d-band (3d in Cu and Zn, 4d in Ag and Cd, and 5d in Au). Besides, Zn and Cd have even lesser PDOS (more than two factors in magnitude than other CF d-band metals) at the Fermi level due to the filling of valence s band as well. Copper has the 3d band centered around its binding energy (E_b) of 3.0–3.5 eV with a d-band width (or range) of ∼ 3 eV [47,48]. Furthermore, Zn and Cd have similar PDOS with localized valence 3d and 4d bands, respectively, centered around the binding energies ∼10 eV [48–50] and ∼11 eV [51,59] below the Fermi level with width ∼ 1.5–2.0 eV. On the other hand, Pd, Ag, and Au have d-band ranges 0–5.5 eV (4d) [53,54], 3.9–7.4 eV (4d) [49], and 2–8 eV (5d) [47,50] below the Fermi level respectively. All DFT approximations agree with each other regarding the shape and width of the d band in the PDOS plot. However, there is a discrepancy in the d-band center (E_b) among them. The PBE-GGA underestimates the binding energy (d-band center) of these metals by ∼ 1–2 eV (maximum for Cd and Zn), whereas SCAN provides a negligible improvement of ∼ 0–0.5 eV upon PBE. On the contrary, the hybrid HSE06 considerably improves on PBE and SCAN by

TABLE III. Formation energies (eV) per atom of alloys other than the B2 phase (CsCl, Pm-3m); CF is completely filled, PF is partially filled.

Alloys	Phase	Combination	PBE	SCAN	HSE06	Expt
AuTi	CuTi (*P*4/*nmm*)	5*d*(CF)-3*d*(PF)	−0.442	−0.630	−0.430	−0.458 ± 0.015 [60]
$ScRh_3$	AuCu3 (*Pm-3m*)	3*d*(PF)-4*d*(PF)	−0.610	−0.762	−0.770	−0.536 ± 0.015 [45]
YPd_3	AuCu3 (*Pm-3m*)	4*d*(PF)-4*d*(CF)	−0.867	−0.890	−1.041	−0.819 ± 0.067 [44]
$ScPt_3$	AuCu3 (*Pm* − 3*m*)	3*d*(PF) − 5*d*(PF)	−1.042	−1.263	−1.173	−0.980 ± 0.021 [61]

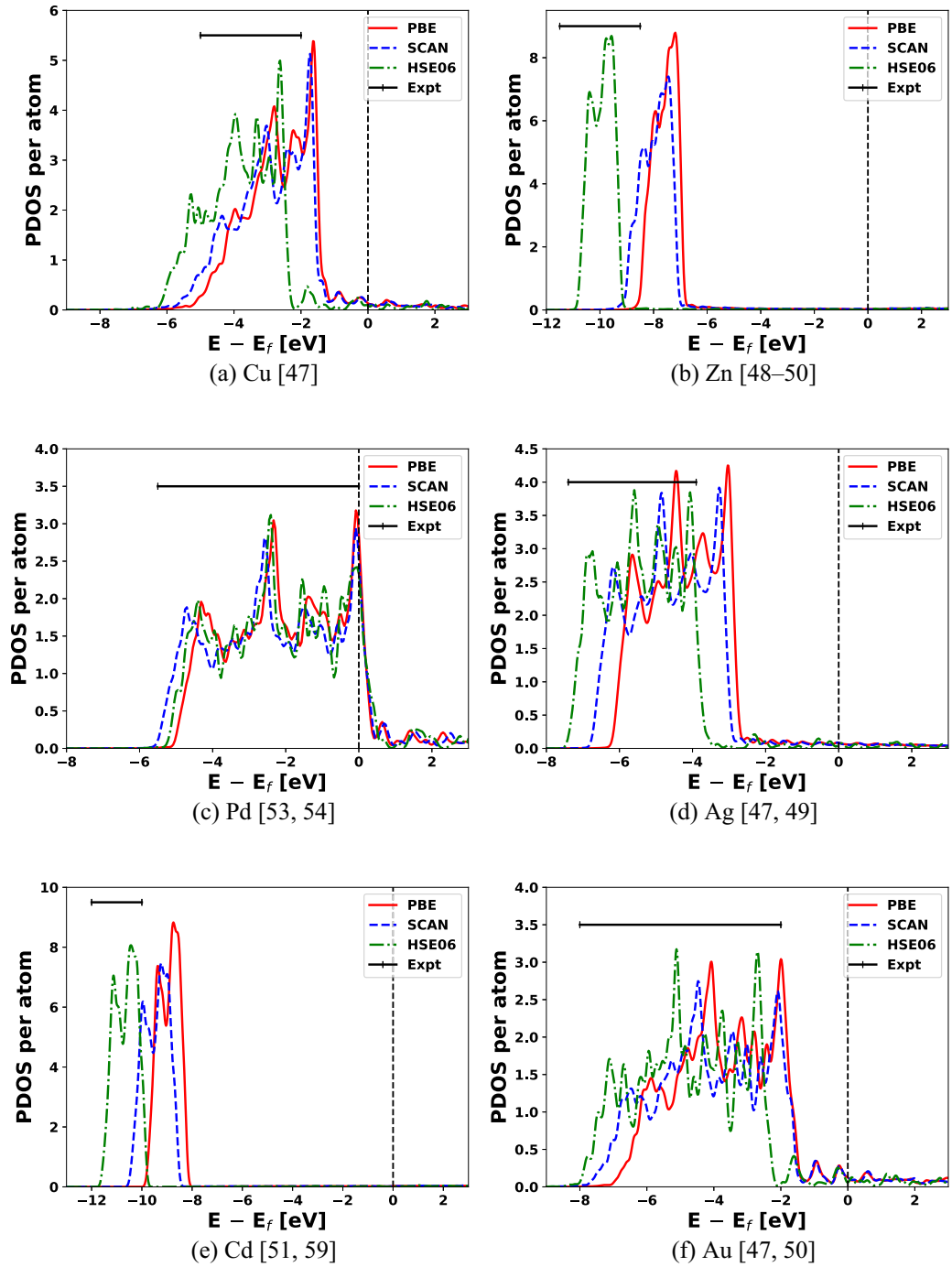

(a) Cu [47] (b) Zn [48–50]

(c) Pd [53, 54] (d) Ag [47, 49]

(e) Cd [51, 59] (f) Au [47, 50]

FIG. 2. The estimated valence d-band density of states with completely filled d configuration compared with valence d-band ranges extracted from experimental x-ray photoemission spectra or ultraviolet photoemission spectra (denoted by horizontal solid line). References are given in subcaptions. ϵ_f is the Fermi level.

increasing the binding energy (blueshifted toward the experimental d-band range) and provides accurate results compared to experiments.

Figure 3 depicts the partial density of states of alloys AgZn [Fig. 3(a)], AgCd [Fig. 3(b)], CuZn [Fig. 3(c)], and AuZn [Fig. 3(d)]. In AgZn, the binding energy of Ag's 4d band increases by $\sim$ 1 eV (onset shifts from 3.0 to 4.0 eV in PBE and SCAN, and 4.0 to 5.0 eV in HSE06) and the width also shrinks by $\sim$ 1 eV compared to pure Ag's 4d band. On the other hand, Zn's 3d band is still localized around almost the same binding energy (small decrement though) as that of the pure Zn, with a negligible decrease in d-band width. These observations are consistent with the experimental results that the 4d band of Ag in AgZn decreases by 1 eV and the width shrinks by 0.7 eV with a negligible effect on the Zn's 3d band compared to its pure constituents [49]. Similar results can be obtained for AgCd, CuZn, and AuZn. Ag's 4d band in AgCd, Cu's 3d band in CuZn, and Au's 5d band in AuZn behave similarly to that of the Ag's 4d band in AgZn. Also, Zn and Cd in these compounds behave likewise as that of Zn in AgZn.

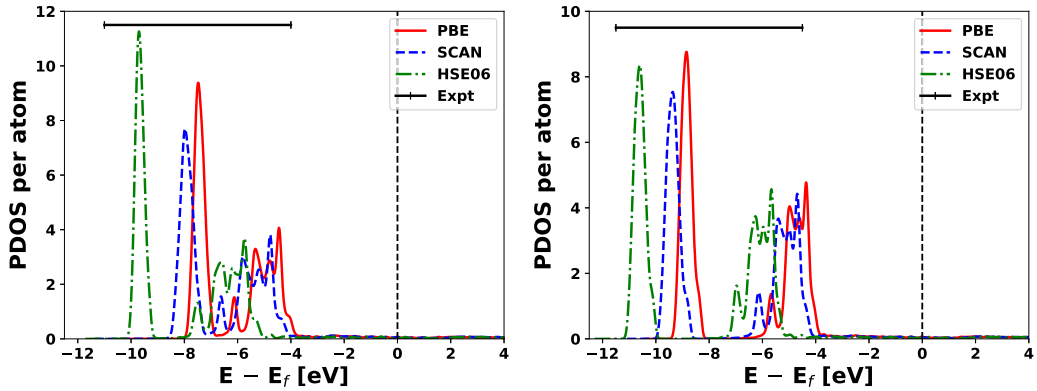

(a) AgZn [49] (b) AgCd [51, 59].

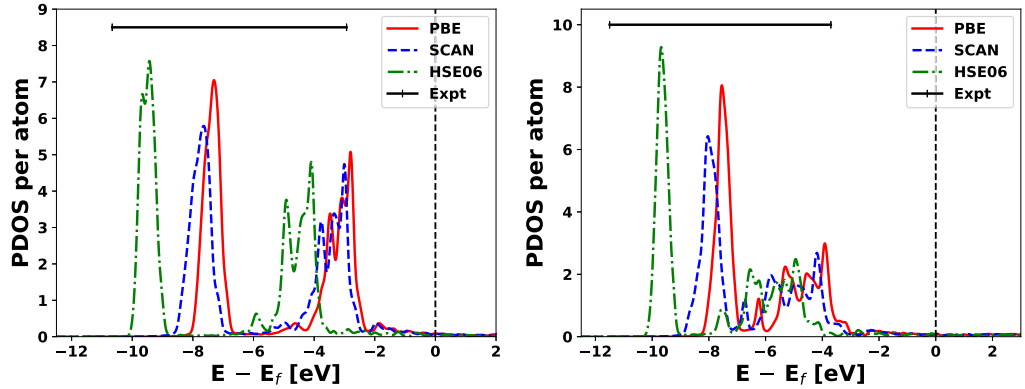

(c) CuZn [48] (d) AuZn [50]

FIG. 3. The estimated valence d-band density of states of alloys with metals having completely filled/completely filled d-band configuration compared with valence d-band ranges extracted from experimental x-ray photoemission spectra or ultraviolet photoemission spectra (denoted by horizontal solid line). References are given in subcaptions. ϵ_f is the Fermi level.

The sharp decrease in d-band widths of Cu, Ag, and Au in alloys can be attributed to the dilution (it increases the distance between two CF metal nearest neighbors, which decreases its overlap with them, thereby giving localized and bound state) of these metals in alloys in presence of more localized 3d and 4d band of Zn and Cd, respectively [48–51]. Also, the increase in binding energy in one of the metals and decrease in binding energy in the other indicates some charge transfer between the constituents [48,50]. Qualitatively, all DFT functionals PBE, SCAN, and HSE06 yield similar results in terms of the change in PDOS of alloys with respect to its constituents. However, only the nonlocal HSE06 provides an accurate binding energy in the case of both alloys and constituents, thereby predicting accurate formation energies. Also, the nonlocal RPA shows similar or better accuracy than that of semilocal functionals in predicting formation energies of CF–CF alloys. We will discuss the RPA results in detail later in a separate section, Failure of RPA and beyond RPA Correction.

B. CF-PF combination

In this section, we discuss the results for alloys with CF-PF d-band combinations such as CuY, ScAg, AgY, AuSc, and ScPd having a B2 phase, as shown in Fig. 1(b). We also present a few other alloys (AuTi and YPd_3) with a different structure than B2 in Table III. The formation energies predicted by PBE-GGA agree well with the experiment, whereas the hybrid HSE06 concurs with PBE for lower formation energies (200–500 meV), while differs significantly from PBE and experimental results in the case of higher formation energies (e.g., YPd_3 and ScPd). On the contrary, SCAN seriously overestimates the formation energies in this region with a decrease in its deviation for alloys with increasing formation energy (YPd_3 and ScPd). The nonlocal RPA consistently overestimates the formation energies of alloys with results closer to SCAN at the best-case scenario.

PDOS of valence d band of partially filled (PF) metals Sc (3d), Y (4d), Rh (4d), Hf (5d), Os (5d), and Pt (5d) are shown in Fig. 4. Unlike the CF metals, there is a significantly large density of states at the Fermi level. Experimentally, both Sc's 3d and Y's 4d band is localized near the Fermi level ($\sim$ 0.2 eV below for Sc) with the d-band widths of $\sim$ 1.5 eV and 2.0 eV respectively [52,57]. Also, Rh's 4d band is concentrated at $\sim$ 1.3–1.5 eV below the Fermi level and has a d-band range of $\sim$ 4.5–5.0 eV [55,62]. The 5d bands of both Hf and Pt have similar localization as that of the 4d band of Rh with centroids around $\sim$ 0.9 eV and $\sim$ 1.6 eV, respectively, with d-band

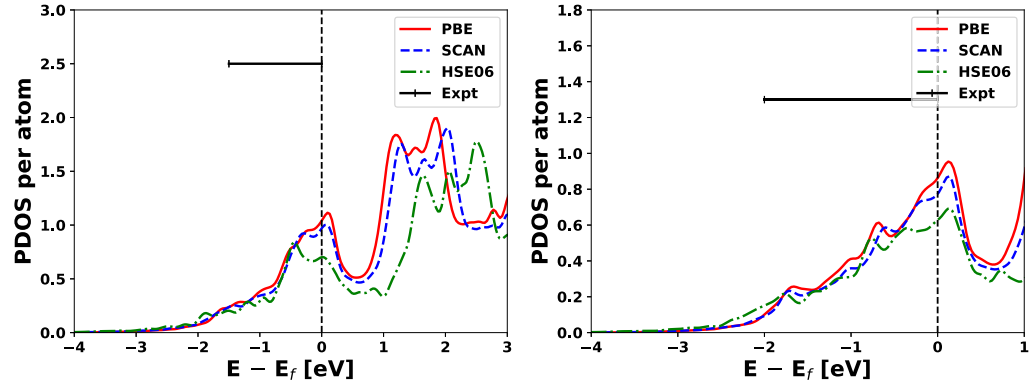

(a) Sc [52] (b) Y [57]

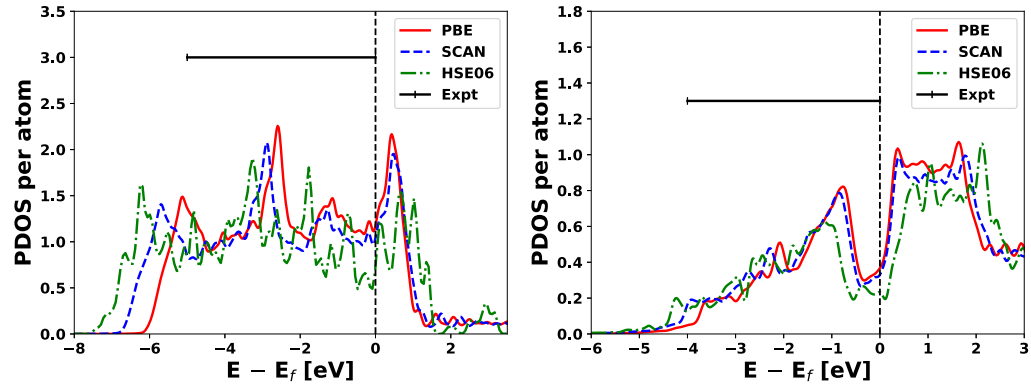

(c) Rh [55, 62] (d) Hf [56]

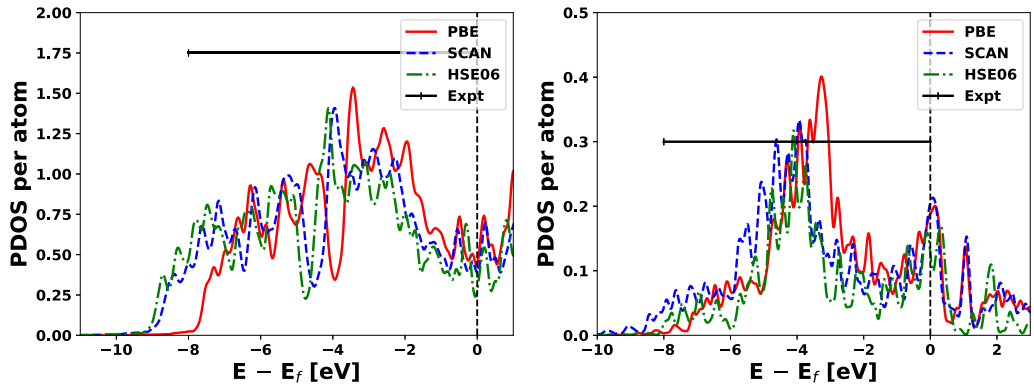

(e) Os [62] (f) Pt [54]

FIG. 4. The estimated valence d-band density of states with partially filled d configuration compared with valence d-band ranges extracted from experimental x-ray photoemission spectra or ultraviolet photoemission spectra (denoted by horizontal solid line). References are given in subcaptions. ϵ_f is the Fermi level.

widths of $\sim$ 4 eV and $\sim$ 8 eV [54,56,62] (Pt's 5d band has two peaks, and it is the first peak). Similary, Os's 5d band has a peak at $\sim$ 3.0 eV and a d-band width of $\sim$ 8.0 eV [62]. For these alloys, the PDOS at the Fermi level decreases as PBE $>$ SCAN $>$ HSE06, except for Pt. Also, the d-band range is blueshifted away from the experimental valence d-band range in the order of PBE $<$ SCAN $<$ HSE06 with PBE being the closest. However, such a shift is noticeable only in the Rh's 4d and Os's 5d bands. Unfortunately, it is difficult to pinpoint the peak or a d-band centroid of DFT calculated PDOS for Rh's 4d, Os's 5d, and Pt's 5d bands, therefore, we could not compare it directly with the experimental values.

Figure 5 shows PDOS results for alloys AgSc, ScPd, and YPd_3. In both ScPd and ScAg, the large density of states at the Fermi level mainly consists of the PF 3d band of Sc,

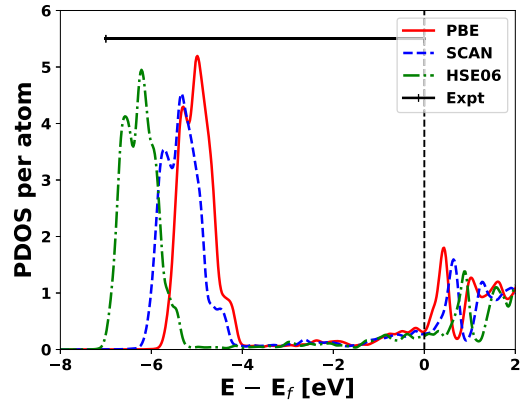

(a) AgSc [52]

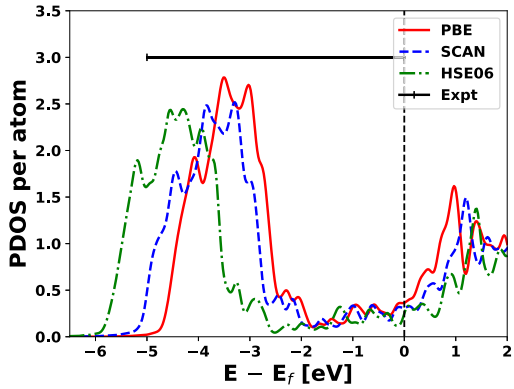

(b) ScPd [52]

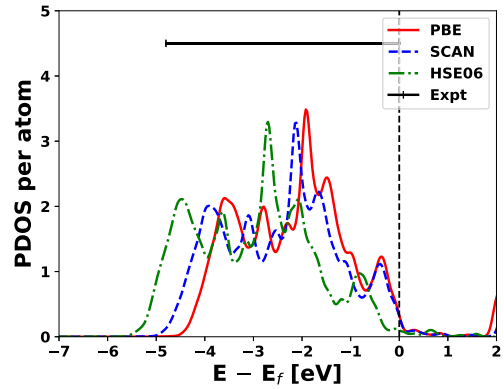

(c) YPd_3 [53, 63]

FIG. 5. The estimated valence d-band density of states of alloys with metals having completely filled/partially filled d-band configuration compared with valence d-band ranges extracted from experimental x-ray photoemission spectra or ultraviolet photoemission spectra (denoted by horizontal solid line). References are given in subcaptions. ϵ_f is the Fermi level.

and its tail is slightly stretched towards larger binding energies compared to its pure counterpart (Sc in ScAg is more stretched than Sc in ScPd) [52]. Our PDOS calculated by all DFT functionals qualitatively agree with this experimental observation [see Figs. 5(a) and 5(b)]. On the other hand, the CF d band of metals Ag and Pd should be redshifted towards a lower binding energy with a decrease in its width due to similar reasons of charge-transfer and dilution as in the case of CF-CF alloys. It is the part where our DFT calculated PDOS differs from the experiment. As expected, PBE underestimates the d-band centroid of the Ag's and Pd's 4d bands, while SCAN slightly blueshifts them. HSE06 also raises the binding energy, however, the shifted 4d band of Ag agrees with the experiment, but is overestimated in the case of Pd's 4d band. This could be the reason that the formation energy predicted by HSE06 is accurate for ScAg, but overestimates the ScPd formation energy. The calculated electronic PDOS of YPd_3 has nonseparable 4d bands of Y and Pd, similar to the experimental photoemission spectrum [53,63]. Nevertheless, it has different centroids and d-band ranges for different DFT methods. Similar to ScPd, the inaccuracy of HSE06 in the prediction of formation energy of YPd_3 is due to an incorrect prediction of the electronic PDOS of an alloy. Conversely, PBE and SCAN provide a reliable estimate of formation energies for both ScPd (Table II), and YPd_3 (Table III), because these functionals predict the correct electronic properties of both alloys and the bulk elements simultaneously.

C. PF-PF combination

Previously, we observed that the inclusion of PF d-band metals in alloys diminish the accuracy of the nonlocal density functionals, while the PBE-GGA consistently outperforms them. The SCAN meta-GGA indeed improves the PBE calculated electronic properties of many alloys and elemental bulks but does not possess similar accuracy in formation energies as that of PBE. Here, we explore the alloys with both PF d-band metals such as HfOs, RhY, ScRh, PtSc, HfPt, $ScRh_3$, and $ScPt_3$. In the PF-PF combination of alloys, both nonlocal functionals, HSE06 and RPA, severely overestimate the formation energies. On the other hand, semilocal functionals perform well with PBE performing much better than the SCAN except for HfPt. Our DFT results show a significant error (overestimation) in the case of HfOs, even for PBE. We suspect that there are some uncertainties in the experiment, as

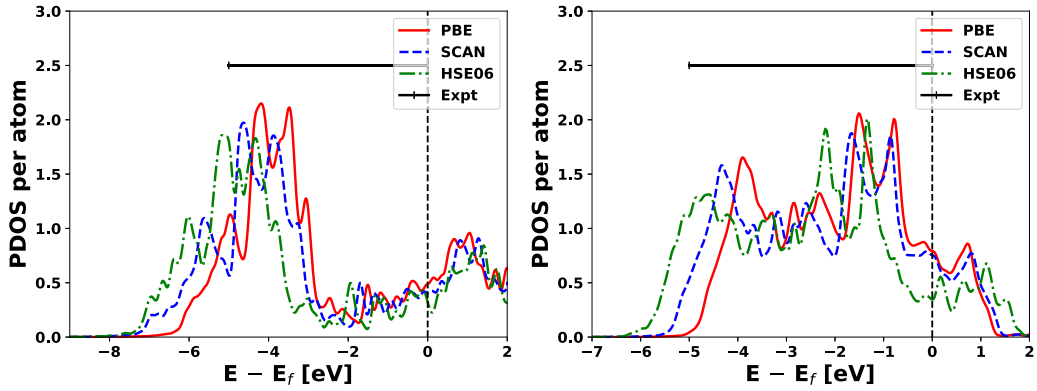

(a) HfPt (b) $ScRh_3$ [58]

FIG. 6. The estimated valence d-band density of states of alloys with metals having partially filled/partially filled d-band configuration compared with valence d-band ranges extracted from experimental x-ray photoemission spectra or ultraviolet photoemission spectra (denoted by horizontal solid line). References are given in subcaptions. ϵ_f is the Fermi level.

a few traces of $Hf_{54}Os_{17}$ and unreacted Os are also present in the sample [43].

In Fig. 6, we compare the PDOS of HfPt [Fig. 6(a)] and $ScRh_3$ [Fig. 6(b)] obtained using various methods. Unfortunately, we could not obtain experimental results for HfPt for comparison but the XPS valence d-band spectra of $ScRh_3$ is available [58]. It has a d band that ranges from the Fermi level to around ~ 5 eV below the Fermi level [58] and it has a shape like that of YPd_3. As expected, HSE06 PDOS is blueshifted away from the experimental range, while PBE and SCAN yield similar PDOS compared to the experiment. However, SCAN overestimates the experimental Rh's $4d$ band width by ~ 1 eV, while the overestimation is only about ~ 0.5 eV in the case of PBE. This result leads to accurate formation energy for the PBE, while SCAN overshoots the experimental value by ~ 230 meV.

Though all DFT-calculated d-band widths of Hf and Pt metals are close to each other and agree with the experiment, we expect that only the SCAN-calculated PDOS of HfPt should be close to that of an experimental result if available, as its formation energies are close to the experimental value.

IV. FAILURE OF RPA AND BEYOND RPA CORRECTION

Earlier, we compared the PBE and SCAN results with HSE06, and established a connection between an accurate prediction of formation energies of alloys and their electronic properties. Here, we discuss the results obtained using the nonlocal RPA. The RPA calculated formation energies of binary alloys in the B2 phase are tabulated in Table II and compared with other semilocal and hybrid functionals as presented in Fig. 1. RPA provides accurate formation energies of CF-CF alloys with a lower energy ($\sim$ $<$ 130 meV) such as for AgZn, AgCd, and CuZn. This is consistent with the previous results for Au–Cu alloys, which have formation energies less than 100 meV [10]. Other CF-CF alloys such as CuPd, AuCd, and AuZn have deviation ranges from 35–50 meV, which is significant as compared to experimental values. Furthermore, errors in RPA enormously increase when an alloy consists of PF d-band metals. In general, it overestimates the experimental formation energies up to the maximum of ~ 350 meV for PtSc.

Though RPA works reasonably well in predicting the cohesive energies of transition metal bulk comparable to PBE [38] with a mean absolute error ~ 0.25 eV, there is a notable difference in the formation energies of alloys. In contrast to formation energy, the cohesive energy of transition metal alloys is a more difficult test for DFT functionals as it involves isolated transition metal atoms [64]. Therefore, more error cancellation is expected for formation energy as both alloys and constituents have the same phase. Here, we have computed the RPA formation energies non-self-consistently using the ground-state PBE eigenstates and eigenvalues as reference. Therefore, we do not have RPA calculated partial density of states to compare with experiment. In RPA, the EXX energy ($E_{\text{total}} - E_c^{\text{RPA}}$) is one-electron self-interaction free, but the correlation energy E_c^{RPA} suffers from a self-correlation error due to the absence of the dynamical exchange-correlation kernel ($f_{xc}(q, \omega)$) [65,66]. RPA provides a good description of the long-range electron-electron correlation required to describe vdW interactions [30,67–69]. However, the short-range electron-electron correlation is not properly described with bare RPA ($f_{\text{xc}} \to 0$) which yields too-negative correlation energies (by ~ 0.4 eV/electron) for the uniform electron gas in the metallic range densities [70,71]. Restoring the nonlocal exchange-correlation kernel can improve the repulsive short-range correlation, thereby giving an exact result [32,70–73]. We suspect that the too-negative formation energies (compared to experiment) by RPA for alloys with PF d-band metals may be related to too-low correlation energy due to an imperfect description of the repulsive short-range electron-electron correlation. Consequently, we computed the formation energies of PtSc and HfOs using the renormalized adiabatic LDA (rALDA) [32,72] and renormalized adiabatic PBE (rAPBE) [73] kernels and tabulated them in Table IV.

The rALDA kernel is obtained by using a (local) truncation of ALDA kernel for wave vector $q > 2k_F$, where $k_F = (3\pi^2 * \text{density})^{1/3}$ is the Fermi wave vector [32,72]. Also, rAPBE is similar to rALDA except it also includes a PBE-like gradient

TABLE IV. Formation energies (eV) per atom from kernel-corrected RPA for PtSc and HfOs. Improving the short-range correlation in RPA can improve the formation energies of intermetallics where RPA fails severely.

	RPA	rALDA	rAPBE	Experiment
HfOs	−0.667	−0.642	−0.612	−0.482 ± 0.052 [12,43][a]
PtSc	−1.440	−1.317	−1.257	−1.086 ± 0.056 [41,45]

[a]It is mentioned in the reference that HfOs alloy sample was not completely pure. It had small amounts of $Hf_{54}Os_{17}$ and relatively important quantities of unreacted Os. Therefore, the true result should be more exothermic than −0.518 eV [43].

correction [73]. A large overestimation of formation energy from RPA can be reduced a little using rALDA. Further, rAPBE improves the RPA formation energies by a significant amount of ∼ 200 meV in the case of PtSc, closer to the experimental value. More corrections in the RPA formation energies can be expected when using a more exact uniform electron gas kernel, such as modified CP07 (MCP07) [71].

V. CONCLUSIONS

We performed DFT calculations to compute the ground-state equilibrium properties of intermetallic alloys. Many earlier studies [5,10] argued that the nonlocality is essential for accurate formation energies. However, those studies covered only a narrow range of WB compounds having CF d-band metals. Our assessment includes a broad range of binary alloys, which also include PF d-band metals. We found that the nonlocality is not always useful for formation energies. Instead, a PBE-like exchange correlation can yield accurate results compared to the experiment, especially for SB intermetallic alloys having PF d-band metals.

Based on the observations, we classified intermetallic alloys into three categories based on their d-band filling combinations, e.g., CF-CF, CF-PF, and PF-PF. The formation energies usually increase in the order of CF-CF < CF-PF < PF-PF. As previously discussed, the nonlocal functionals HSE06 and RPA give accurate formation energies of CF-CF alloys, while PBE-GGA yields better results in the case of CF-PF and PF-PF alloys. Therefore, we suggest using a more PBE-like exchange correlation for SB alloys having a PF d-band metal, while the nonlocality is necessary to capture the energy differences in the case of WB alloys with CF d-band transition metals. The difficulties to incorporate a delicate balance between two such extreme cases make it arduous for any DFT approximation to provide the accurate equilibrium properties of a wide range of alloys. Nevertheless, a meta-GGA could be a natural trade-off, as it contains some nonlocality due to the kinetic energy density, while it still maintains its status as a semilocal approximation.

In addition, we also established a one-to-one correspondence between formation energies and electronic properties by estimating the d-band contribution to valence DOS. In other words, the functional which predicts accurate PDOS of alloys and metals simultaneously also agrees with the experimental formation energies. The PBE-GGA underestimates the d-band range of CF transition metals and their alloys while it provides electronic PDOS often similar or better than HSE06 in the case of PF d-band metals and their alloys. Contrarily, SCAN often improves on PBE-calculated d-band centroid and hence the d-band range of many alloys and bulk metals, but it does not share similar success as that of PBE. It may be due to a lack of required error cancellation in the SCAN meta-GGA that should be expected due to the same phase of the alloy and its constituents.

The state-of-the-art RPA, which can describe different bonding situations often much better than semilocal and hybrid functionals, severely fails for the formation energies of intermetallic alloys with PF d-band metals. It significantly overestimates the formation energies. This may be related to the too-negative correlation energies within the metallic densities due to the incomplete description of repulsive short-range electron-electron correlations. Restoring the nonlocal exchange-correlation kernel rAPBE improves the formation energy of PtSc by ∼ 200 meV, which is substantial. The experimental formation energy of some alloys are either limited in number or unavailable and also accompanied by an error bar. However, those error bars are four- to five fold smaller than the actual functional error. Therefore, our overall conclusions about the performance of various density functionals remain valid, in a qualitative sense, even for those alloys. Also, in the absence of experimental results for many alloys, there is a strong need for more robust theoretical methods. One direction could be to look at the kernel-corrected RPA using the modified CP07 (MCP07) kernel [70] of the uniform electron gas. It satisfies all the exact constraints that a complex kernel with the real frequency can satisfy for that model of a metal.

ACKNOWLEDGMENTS

N.K.N. and A.R. acknowledge support by the National Science Foundation under Grant No. DMR-1553022. Computational support was provided by Temple University's HPC resources and thus was supported in part by the National Science Foundation through major research instrumentation Grant No. 1625061 and by the US Army Research Laboratory under Contract No. W911NF-16-2-0189. The work of S.A. was supported by the US Department of Energy, Office of Sciences, Office of Basic Energy Sciences as part of the Computational Chemical Sciences Program under Award No. DE-SC0018331. The work of B.N. was supported as part of the Center of Complex Materials from First Principles (CCM), an Energy Frontier Research Center funded by the US Department of Energy (DOE), Office of Science, Basic Energy Sciences (BES), under Award No. DE-SC0012575.

[1] W. Pfeiler, *Alloy Physics: A Comprehensive Reference* (John Wiley & Sons, Germany, 2007).

[2] E. Mooser and W. Pearson, Acta Crystallogr. **12**, 1015 (1959).

[3] F. Stein, M. Palm, and G. Sauthoff, Intermetallics **12**, 713 (2004).

[4] F. E. Wang, *Bonding Theory for Metals and Alloys* (Elsevier, Netherlands, 2018).

[5] Y. Zhang, G. Kresse, and C. Wolverton, Phys. Rev. Lett. **112**, 075502 (2014).

[6] P. Hohenberg and W. Kohn, Phys. Rev. **136**, B864 (1964).

[7] W. Kohn and L. J. Sham, Phys. Rev. **140**, A1133 (1965).

[8] V. Ozoliņš, C. Wolverton, and A. Zunger, Phys. Rev. B **57**, 6427 (1998).

[9] L.-Y. Tian, H. Levämäki, M. Ropo, K. Kokko, Á. Nagy, and L. Vitos, Phys. Rev. Lett. **117**, 066401 (2016).

[10] N. K. Nepal, S. Adhikari, J. E. Bates, and A. Ruzsinszky, Phys. Rev. B **100**, 045135 (2019).

[11] J. P. Perdew, K. Burke, and M. Ernzerhof, Phys. Rev. Lett. **77**, 3865 (1996).

[12] E. B. Isaacs and C. Wolverton, Phys. Rev. Mater. **2**, 063801 (2018).

[13] P. Janthon, S. Luo, S. M. Kozlov, F. Vines, J. Limtrakul, D. G. Truhlar, and F. Illas, J Chem. Theory Comput. **10**, 3832 (2014).

[14] J. Heyd, G. E. Scuseria, and M. Ernzerhof, J. Chem. Phys. **118**, 8207 (2003).

[15] J. Heyd, G. E. Scuseria, and M. Ernzerhof, J. Chem. Phys. **124**, 219906 (2006).

[16] D. Pines and D. Bohm, Phys. Rev. **85**, 338 (1952).

[17] D. Bohm and D. Pines, Phys. Rev. **92**, 609 (1953).

[18] D. C. Langreth and J. P. Perdew, Phys. Rev. B **21**, 5469 (1980).

[19] D. C. Langreth and J. P. Perdew, Solid State Commun. **17**, 1425 (1975).

[20] D. C. Langreth and J. P. Perdew, Phys. Rev. B **15**, 2884 (1977).

[21] R. Zhang, S. Sheng, and B. Liu, Chem. Phys. Lett. **442**, 511 (2007).

[22] J. P. Perdew and K. Schmidt, in *Density Functional Theory and Its Applications to Materials*, edited by V. Van Doren, C. Van Alsenoy, and P. Geerlings, AIP Conf. Proc. No. 577 (AIP Conference Proceedings, Melville, NY, 2001), pp. 1–20.

[23] J. Sun, A. Ruzsinszky, and J. P. Perdew, Phys. Rev. Lett. **115**, 036402 (2015).

[24] P. E. Blöchl, Phys. Rev. B **50**, 17953 (1994).

[25] J. Hafner, J. Comput. Chem. **29**, 2044 (2008).

[26] M. Walter, H. Häkkinen, L. Lehtovaara, M. Puska, J. Enkovaara, C. Rostgaard, and J. J. Mortensen, J. Chem. Phys. **128**, 244101 (2008).

[27] J. J. Mortensen, L. B. Hansen, and K. W. Jacobsen, Phys. Rev. B **71**, 035109 (2005).

[28] S. R. Bahn and K. W. Jacobsen, Comput. Sci. Eng. **4**, 56 (2002).

[29] See Supplemental Material at http://link.aps.org/supplemental/10.1103/PhysRevB.102.205121 for a PDF with data tables and figures referenced in the main text, which includes Refs. [74–78].

[30] J. Harl and G. Kresse, Phys. Rev. B **77**, 045136 (2008).

[31] C. E. Patrick and K. S. Thygesen, J. Chem. Phys. **143**, 102802 (2015).

[32] T. Olsen and K. S. Thygesen, Phys. Rev. B **87**, 075111 (2013).

[33] J. Harl, L. Schimka, and G. Kresse, Phys. Rev. B **81**, 115126 (2010).

[34] G. Kresse and D. Joubert, Phys. Rev. B **59**, 1758 (1999).

[35] F. Birch, Phys. Rev. **71**, 809 (1947).

[36] T. Massalski, H. Okamoto, L. Kacprzak, and P. Subramanian, *Binary Alloy Phase Diagrams, plus Updates* (ASM International, Materials Park, OH, 1996).

[37] V. N. Staroverov, G. E. Scuseria, J. Tao, and J. P. Perdew, Phys. Rev. B **69**, 075102 (2004).

[38] L. Schimka, R. Gaudoin, J. Klimeš, M. Marsman, and G. Kresse, Phys. Rev. B **87**, 214102 (2013).

[39] R. Hultgren, P. D. Desai, D. T. Hawkins, M. Gleiser, and K. K. Kelley, *Selected Values of the Thermodynamic Properties of Binary Alloys*, National Standard Reference Data System, (John Wiley & Sons Inc., USA, 1973.

[40] S. Watanabe and O. Kleppa, Metall. Trans. B **15**, 357 (1984).

[41] Q. Guo and O. J. Kleppa, J. Alloys Compd. **321**, 169 (2001).

[42] K. Fitzner, W.-G. Jung, and O. Kleppa, Metall. Trans. A **22**, 1103 (1991).

[43] K. Mahdouk and J.-C. Gachon, J. Alloys Compd. **278**, 185 (1998).

[44] N. Selhaoui and O. Kleppa, J. Chem. Phys. **90**, 435 (1993).

[45] N. Selhaoui and O. Kleppa, J. Alloys Compd. **191**, 145 (1993).

[46] L. Topor and O. Kleppa, Metall. Trans. A **19**, 1827 (1988).

[47] D. Eastman and J. Cashion, Phys. Rev. Lett. **24**, 310 (1970).

[48] P. Andrews and L. Hisscott, J. Phys. F Met. Phys. **5**, 1568 (1975).

[49] R. Jordan, D. Zehner, N. Harrison, P. Durham, and W. Temmerman, Z. Phys., B, Condens. Matter. **75**, 291 (1989).

[50] J. Leiro, K. Kokko, and R. Laihia, J. Electron Spectrosc. **113**, 167 (2001).

[51] J. Riley, R. Leckey, J. Jenkin, J. Liesegang, and R. Poole, J. Phys. F: Met. Phys. **6**, 293 (1976).

[52] F. Battye, H. Schulz, A. Goldmann, S. Hufner, D. Seipler, and B. Elschner, J. Phys. F: Met. Phys. **8**, 709 (1978).

[53] J. C. Fuggle, F. U. Hillebrecht, R. Zeller, Z. Zołnierek, P. A. Bennett, and C. Freiburg, Phys. Rev. B **27**, 2145 (1983).

[54] H. Höchst, S. Hüfner, and A. Goldmann, Phys. Lett. A **57**, 265 (1976).

[55] J. W. Niemantsverdriet, *Spectroscopy in Catalysis: An Introduction* (John Wiley & Sons, 2007).

[56] P. Steiner, H. Höchst, J. Schneider, S. Hüfner, and C. Politis, Z. Phys. B: Condens. Matter. **33**, 241 (1979).

[57] A. Fujimori and L. Schlapbach, J. Phys. C: Solid State Phys. **17**, 341 (1984).

[58] M. Oku, T. Shishido, T. Shinohara, T. Fukuda, Q. Sun, Y. Kawazoe, and K. Wagatsuma, J. Alloys Compd. **339**, 317 (2002).

[59] G. Crecelius and G. K. Wertheim, Phys. Rev. B **18**, 6525 (1978).

[60] K. Fitzner and O. Kleppa, Metall. Mater. Trans. A **23**, 997 (1992).

[61] Q. Guo and O. Kleppa, J. Phys. Chem. **99**, 2854 (1995).

[62] C. Fadley and D. Shirley, J. Res. Natl. Bur. Stand., Sect. A **74**, 543 (1970).

[63] E. Vogelzang, M. Sikkens, and G. Sawatzky, Sol. Energy Mater. **14**, 365 (1986).

[64] C. J. Cramer and D. G. Truhlar, Phys. Chem. Chem. Phys. **11**, 10757 (2009).

[65] H. Eshuis, J. E. Bates, and F. Furche, Theor. Chem. Acc. **131**, 1084 (2012).

[66] X. Ren, P. Rinke, C. Joas, and M. Scheffler, J. Mater. Sci. **47**, 7447 (2012).
[67] L. Schimka, J. Harl, A. Stroppa, A. Grüneis, M. Marsman, F. Mittendorfer, and G. Kresse, Nat. Mater. **9**, 741 (2010).
[68] T. Björkman, A. Gulans, A. V. Krasheninnikov, and R. M. Nieminen, Phys. Rev. Lett. **108**, 235502 (2012).
[69] N. K. Nepal, A. Ruzsinszky, and J. E. Bates, Phys. Rev. B **97**, 115140 (2018).
[70] M. Lein, E. K. U. Gross, and J. P. Perdew, Phys. Rev. B **61**, 13431 (2000).
[71] A. Ruzsinszky, N. K. Nepal, J. M. Pitarke, and J. P. Perdew, Phys. Rev. B **101**, 245135 (2020).
[72] T. Olsen and K. S. Thygesen, Phys. Rev. B **86**, 081103(R) (2012).
[73] T. Olsen and K. S. Thygesen, Phys. Rev. Lett. **112**, 203001 (2014).
[74] D. Lazarus, Phys. Rev. **76**, 545 (1949).
[75] N. Nakanishi, T. Mori, S. Miura, Y. Murakami, and S. Kachi, Philos. Mag. **28**, 277 (1973).
[76] V. S. Guthikonda and R. S. Elliott, Continuum Mech. Thermodyn. **21**, 269 (2009).
[77] J. R. Morris, Y. Ye, Y.-B. Lee, B. N. Harmon, K. A. Gschneidner, Jr., and A. M. Russell, Acta Mater. **52**, 4849 (2004).
[78] S. Zirinsky, Acta Metall. **4**, 164 (1956).